Journal of Energy Storage 58 (2023) 106316

Contents lists available at ScienceDirect

Journal of Energy Storage

journal homepage: www.elsevier.com/locate/est

Research papers

Robust synergistic effect of TiS_2/MoS_2 hierarchal micro-flowers composite realizing enhanced electrochemical performance

Ghulam Nabi [a,b,*], Wajid Ali [a], Muhammad Tanveer [a,**], Tahir Iqbal [a], Muhammad Rizwan [c], S. Hussain [d]

[a] Department of Physics, University of Gujrat, Gujrat 50700, Pakistan
[b] Institute of Physics, Technical University of Ilmenau, Ilmenau 98693, Germany
[c] School of Physical Sciences, University of the Punjab, Lahore, Pakistan
[d] Department of Physics, Division of Science and Technology, University of Education, Lahore, Pakistan

ARTICLE INFO

Keywords:
TiS_2/MoS_2
Binary composites
Hierarchical micro-spheres
Specific capacitance

ABSTRACT

Currently, development of efficient binary composite electrode materials is a dire need to overcome the energy crises globally. Determent to increase the capacitance of supercapacitor, TiS_2, MoS_2 and TiS_2/MoS_2 composites are synthesized by hydrothermal technique and their growth mechanism is also proposed. The structural and morphological properties of the grown materials were examined by employing SEM, EDS, XRD and TEM techniques. In synthesized hierarchal micro-flowers composite the nano-sheets are evenly distributed on the spherical surface improving the surface porosity and surface area resulting enhancement in the electrons and ions transfer on the TiS_2/MoS_2 surface. The TiS_2/MoS_2 composite based electrode exhibited significantly improved specific capacitance (709 F/g) in contrast to individual TiS_2 (480 F/g) and MoS_2 (402 F/g) owing to their fast ion transfer, numerous active sites on their high surface area and robust synergistic effect. Additionally, after 4000 cycles, more than 91 % capacitance was sustained for TiS_2/MoS_2 composite indicating their excellent stability. Consequently, TiS_2/MoS_2 binary metal sulfide composites with enhanced specific capacitance and significantly extended cycle life validating their potential applications in high-performance energy storage devices.

1. Introduction

Research scientists are working on the development of efficient, reliable, cost effective, light weight and adaptable energy storage devices to meet the growing energy demand globally [1,2]. Considering these aspects, researchers are conducting extensive research on batteries and electrochemical capacitors which are recognized as important energy storage devices. [3,4]. Batteries have less power density but higher energy density. The key objective is to approach superior power density and energy density to boost the capabilities of supercapacitors and batteries [5,6]. Therefore to improve the proficiency of energy storage systems, the world is shifting toward emerging supercapacitor owing to significantly high energy and power densities, comprehensive cyclic stability, light weight and thermal stability at to extremely high temperatures [7–10].

Supercapacitors are consistently termed as ultra-capacitors and electric double layer capacitors (EDLCs) having significantly higher power and energy densities in comparison with conventional capacitors [11–13]. The ultra-capacitors have surprisingly less internal resistance and longer cycle life [13]. Supercapacitors are commonly employed in a variety of fields such as electric vehicles, consumer electronics, low power devices, photovoltaic systems, microcomputers and to stabilize the power supply [11–14]. Supercapacitors are categorized into various types depending upon their charge storing methods [15,16]. Whenever an electrical high voltage is applied to an EDLC, it uses non-faradic processes to form a Helmholtz layer [16–18]. The second type is pseudocapacitors that operates on faradic reactions and chemical absorbance on their electrode surface. Finally, there is a hybrid capacitor that can operate on both anodic and non-faradic processes. [19–21].

The most advanced sort of supercapacitor is the hybrid supercapacitor [22–24]. Carbon electrodes are utilized in double layer capacitors, which shows a less energy density problems [25–27]. Pseudocapacitors, on the other hand, used metal oxide or conducting polymers as the electrode, which has comparatively lower power density

* Correspondence to: G. Nabi, Department of Physics, University of Gujrat, Gujrat 50700, Pakistan.
** Corresponding author.
E-mail addresses: gnwattoo@uog.edu.pk (G. Nabi), dr.tanveer@uog.edu.pk (M. Tanveer).

https://doi.org/10.1016/j.est.2022.106316
Received 28 September 2022; Received in revised form 19 November 2022; Accepted 3 December 2022
Available online 14 December 2022

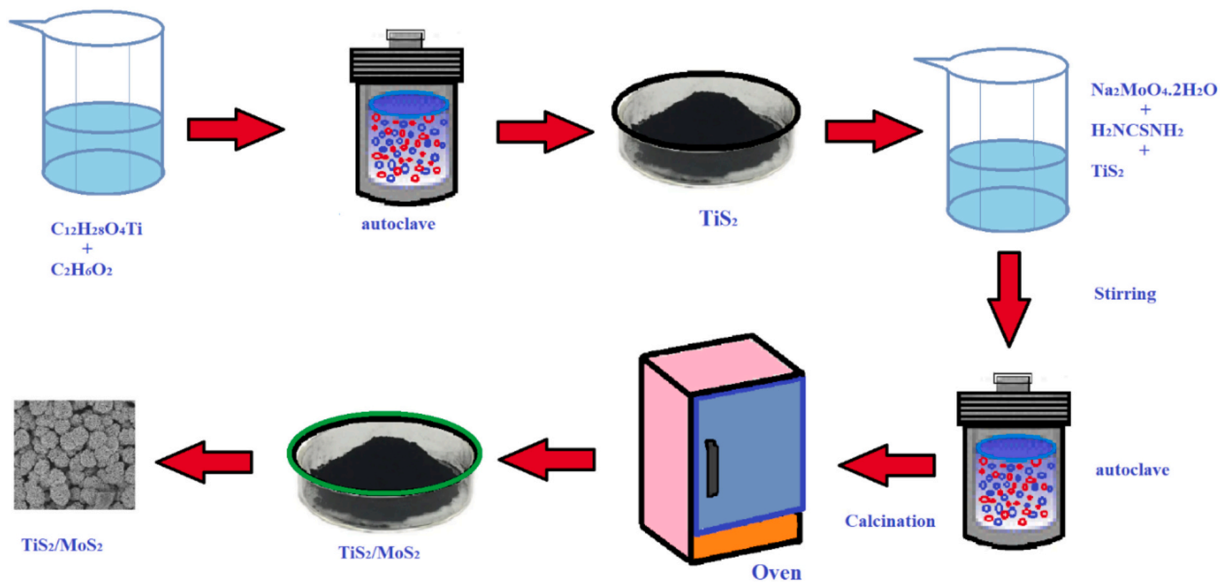

Fig. 1. Schematic diagram of TiS_2/MoS_2 hierarchal micro-flowers composite synthesis.

but greater energy density [23,28,29]. Careful literature review depicts that numerous materials including metal oxide, semi metal sulfides (MoS_2 and VS_2), semi-conductors (TiS_2 and WS_2), transition metal dichalcogenides, and superconductors (niobium selinide) have been used for supercapacitor applications [30,31]. Researchers are working on newly developed metal dichalcogenides based 2D semiconductor materials such as molybdenum sulfide nano-sheets as electrodes for supercapacitor applications, [32,33]. Sulfide compounds exhibit two or more valence states which leads to the high specific capacitance [34–36]. Many sulfide and oxide nanomaterials have recently been employed as electrode materials in supercapacitor applications such as ZnS [37], CuS [38], CuO [39] and NiS [40] due to their reasonable specific capacitance.

Recent research on TiS_2 exposes that it has a specific capacitance near 4.60 F/g without use of binder and conductive carbon black. Afterwards by mixing binder and conductive carbon black its capacitance enhances to 195 F/g having working potential window up to 3 V. This proves that carbon may be utilized to enhance the conduction of metal sulfides and transition metal oxides for prospective uses in supercapacitors [41–43]. Furthermore, various doped materials have been synthesized to enhance the efficiency of supercapacitors including Ti-doped $Na_4Mn_9O_{18}$ [44], Ti-Doped Fe_2O_3 [45], Ti-doped V_2O_5 [46], Mo-doped ZnO [47] and S-doped CoP [48]. Presently, significant enhancement in the efficiency of supercapacitors have been attained by various hybrid composite material containing g-C_3N_4/MnO_2 [49], NiS_2@MoS_2, TiS_2/g-C_3N_4 [50], AC/TiS_2 [51], NTs/MoS_2 [52], AC/MoS_2 [53], MoS_2/TiO_2 [54], NTs/MoS_2 [54] and MoS_2/PPy-2 [54].

Previous literature review depicts that various effective methods are being used in order to improve the performance of supercapacitors including (i) tuning of morphology (ii) addition of carbon black (iii) transition metal doping and (iv) composites assembling are most significant. Among these methods composites are frequently employed in energy storage systems owing to outstanding characteristics covering easy ion transfer, low resistance, low erosion, high electrical conductivity and high cyclic stability along with high thermal stability [55–57]. Composite materials consist of various secondary phases which play significant role in improving its electrochemical performance synergistically contrary to the dopant material wherein various doped element are presented in the crystal structure of the host substance lattices preserving its basic structure [58–61]. Titanium disulfide (TiS_2) is an inorganic substance with hexagonal structure. Similarly, MoS_2 is also an inorganic substance having identical hexagonal structures. So, these symmetrically identical structures and having crucial properties maybe a decent choice for the hybrid composites TiS_2/MoS_2 [62].

Motivated by their superior characteristics, identical structures and composites synergistic performance, here, TiS_2, MoS_2 and their composite (TiS_2\$MoS_2$) has been synthesized for the first time for their enhanced electrochemical performance. With the composition of TiS_2/MoS_2 based electrode exhibited significantly improved specific capacitance (709 F/g) as compared to individual TiS_2 (480 F/g) and MoS_2 (402 F/g) owing to their uniform hierarchical micro-structures growth, fast ion transfer, numerous active sites on their high surface area and robust synergistic effect. Reported composite TiS_2\$MoS_2$ exhibited 32 % improvement w.r.t. TiS_2 and 43.3 % improvement w.r.t. MoS_2. Additionally, after 4000 cycles, more than 91 % capacitance was sustained by TiS_2/MoS_2, composite indicating their excellent stability. So, the as synthesized TiS_2/MoS_2 binary metal sulfides composite with considerably improved specific capacitance and extended cycle life validating their potential utilization as electrode materials for sophisticated energy storage devices.

2. Experimental

2.1. Materials

Analytical grade precursors, titanium isopropoxide ($C_{12}H_{28}O_4$Ti-97 %), ethylene glycol ($C_2H_6O_2$–99.8 %), ethanol (C_2H_6O-99.8 %), Cetyl Trimethyl Ammonium Bromide ($C_{19}H_{42}$BrN-98 %), thio-urea and ($Na_2MoO_4.2H_2O$-97 %) were bought from the Sigma-Aldrich.

2.2. Pristine titanium disulfide (TiS_2) synthesis

Firstly, a thio-urea solution was prepared in 20 ml of de-ionized H_2O. Room temperature stirring was done for 2 h. Another solution was made by combining 10 ml $C_{12}H_{28}O_4$Ti and 1 ml $C_2H_6O_2$ which used as a binder include and then vigorously stirred it for 2 h. Later on, both prepared solutions were blended to form a homogeneous solution and put it into autoclave. Then the autoclave was placed into the muffle furnace and heated at 180 °C for 18 h. After reaction completion, the autoclave was naturally cooled to room temperature. Finally, the obtain precipitates were washed with ethanol. After drying the precipitate for 7 h at 280 °C, undoped titanium disulfide (TiS_2) powder form was achieved.

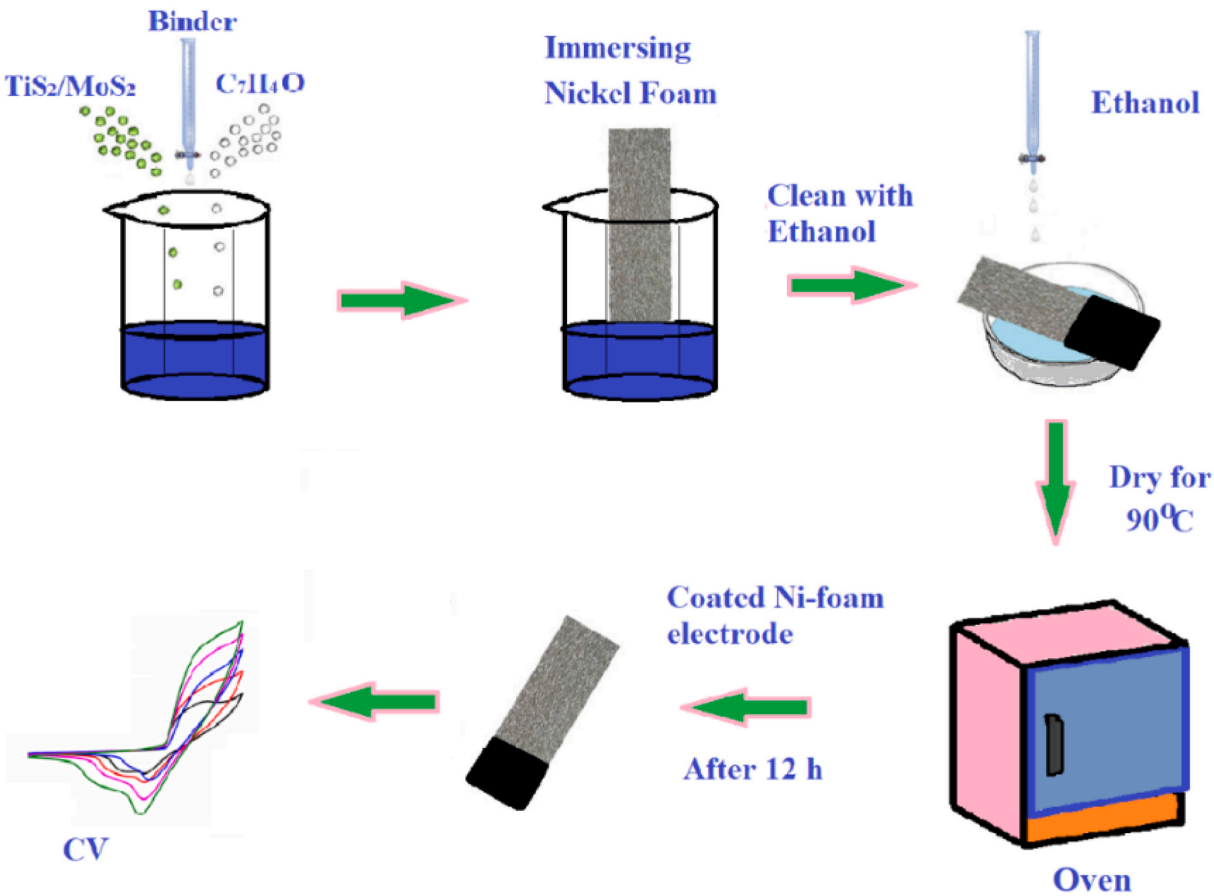

Fig. 2. Systematic schematic diagram of prepared electrode.

2.3. Pristine molybdenum disulfide (MoS_2) synthesis

The MoS_2 structures were synthesized by using hydrothermal method. In in 80 ml water, 2.14 g $Na_2MoO_4.2H_2O$ and 2.06 g H_2NCSNH_2 were added and continuously stirred for 1 h. The pH was maintained less than 10 with 11.12 M HCl. The prepared mixture was put into the 100 ml stainless teflon autoclave and temperature was adjusted at 160 °C for 18 h. Laterally, the completion of reaction, the black-brown MoS_2 precipitates were collected through filtration. The product was washed a number of times with ethanol and H_2O numerous times.

2.4. Hybrid composite (TiS_2/MoS_2) synthesis

The synergetic combinations of hexagonal titanium disulfide (TiS_2) and hexagonal plane molybdenum disulfide (MoS_2) has been obtained by simple facile hydrothermal technique. Firstly, prepared the homogeneous solution of TiS_2 in 20 ml of distilled water and then precisely added molybdenum disulfide (MoS_2). After this addition it was stirred continuously for 3 h at the room temperature and during stirring added CTAB to ensure slow hydrolysis process. Then this prepared liquid solution was added in stainless autoclave and placed in heating furnace whose temperature was adjusted at the temperature 180 °C for 24 h. Subsequently to reaction completion, teflon autoclave was self-cooled to room temperature. After cooling, the attained product was washed numerous times with ethanol and H_2O then calcined it at 550 °C for 2 h. The schematic illustrations of the controlled synthesis process of hierarchal micro-flowers is revealed in the Fig. 1.

2.5. Materials characterization

The obtained products were studied by X-ray diffractometer (XRD) using its parameters such as radiation source of Cu-Kα (λ = 1.54056 Å). The scanning electron microscopy (SEM) was done by using Hitachi S-4800. Hitachi S-4800 was also fitted with energy dispersive x-rays spectroscopy for the elemental analysis. The JEOL JEM-2100 (Japan) has been used for transmission electron microscopy (TEM). Gamry-5000E, (Made in USA) potentiostat was used to analyze the electrochemical performance of pristine and composites material.

2.6. Electrochemical measurements

The electrochemical performance has been tested in a 2 M KOH electrolyte by applying the three electrode setup. The composition of the electrode preparation was ordered as 80 % (0.25 mg) synthesized materials TiS2/MoS2, 15 % (0.3 mg) carbon black (weight percentage) as a conduction substantial, and in last 5 % (0.2 mg) binder Polytetrafluoroethylene (PTFE). This slurry solution was applied to nickel foam (1 cm × 1 cm) area. Finally, the prepared electrode was dried at 85 oC for almost 12 h in the muffle furnace. Then cyclic voltammetry (CV), galvanometric charge discharge (GCD) and electrochemical impedance spectroscopy (EIS) were evaluated at various parameters by using the Gamry 5000E electrochemical workstation as illustrated in the Fig. 2.

Specific capacitance (Cs) of synthesized electrode were estimated by employing cyclic voltammetry equations in Eqs. (1) and (2) [50,63]:

$$Cs = \frac{\int Idv}{Mv\Delta V} \quad (1)$$

Whereas ΔV denotes the scan rate (mVs^{-1}), M belongs to active mass in (mg), I refer the current in (mA) and V_i and V_f is potential window which is also called initial and final voltages respectively.

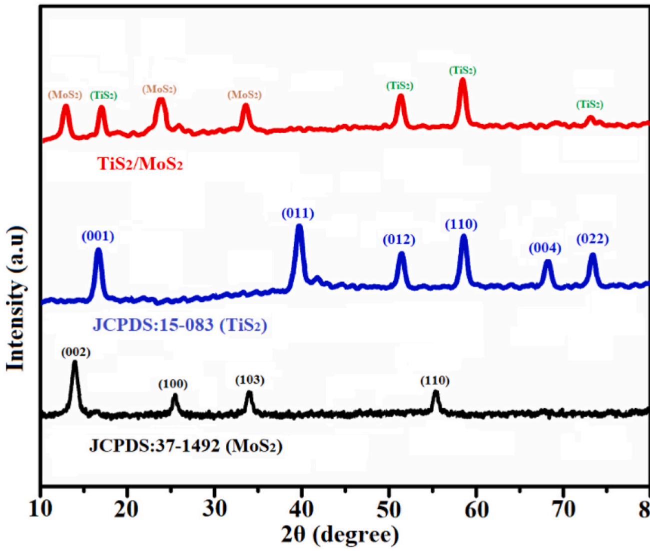

Fig. 3. XRD Pattern of TiS_2, MoS_2 and TiS_2 / MoS_2 hierarchal micro-flowers composite.

$$Cs = \frac{I \times \Delta t}{\Delta V \times M} \quad (2)$$

Whereas M refers to the active mass (mg), which is pasted on nickel foam (1 cm × 1 cm) area, I refer to applied current (mA), ΔV belongs potential window and Δt belongs to discharging time.

3. Results and discussion

By using XRD approach the size, crystallographic structure and phase structures of synthesized materials were analyzed. As it can be seen in the Fig. 3, the diffraction peaks at 2θ = 12.1°, 25.7, 35° and 58.3° corresponding to the hkl planes (002) (100) (103) and (110) consistent with MoS_2 (JCPDS no. 37–1492). Their crystal structure is hexagonal having space group hP6, $P6_3/mmc$, No. 194 and density (ρ) 5.06 g/cm^3. The lattice parameters of MoS_2 are as, a = 3.161 Å, b = 3.161 Å and c = 12.295 Å.

The XRD analysis of TiS_2 shows that the intensity peaks are at 2θ = 16.3°, 44.7°, 53.5°, 60.2°, 68.9° and 75.4° respectively match well with hkl diffraction planes (001), (011), (012) (1100), (004) and (002). These diffraction planes of TiS_2 are consistent with the JCPDS no. 15–083 of TiS_2. The TiS_2 has hexagonal structure with space group P-3 m1 No. 164 and density (ρ) 3.22 g/cm^3. The lattice parameters if TiS_2 are, a = 3.42 Å, b = 3.42 Å and c = 5.72 Å with, α = 90°, β = 90°, γ = 120°. MoS_2 diffraction peaks are comparatively weak and narrow, in contrast to TiS_2 weak but both are showing crystalline nature. The XRD pattern of the TiS_2/MoS_2 composite samples was also characterize which revealed the successful synthesis and crystalline nature of the product. Furthermore, the crystalline peak formation of the composites is almost identical, indicating that the molar ratio of Ti and Mo has minimal influence on the crystal structure as depicted in the Fig. 3. All the XRD peaks show the successful growth of the samples which were further characterized and utilized for electrode materials.

SEM and TEM have been employed to examine the morphological structures, size and shape of prepared materials as displayed in the Figs. 4 and 5. The SEM of pristine TiS_2 clearly showing the nanorods having width in 100–200 nm whereas their length is in the range of 400–600 nm as depicted in the Fig. 4 (a). The shape of the these nanorods is resembling with each other and apparently no much difference have been found between these rods. The pattern of these nanorods is smooth and regular. Energy dispersive X-rays spectroscopy was used for the elemental analysis. The elemental analysis showing that the synthesized material consists of Ti and S without any impurity as depicted

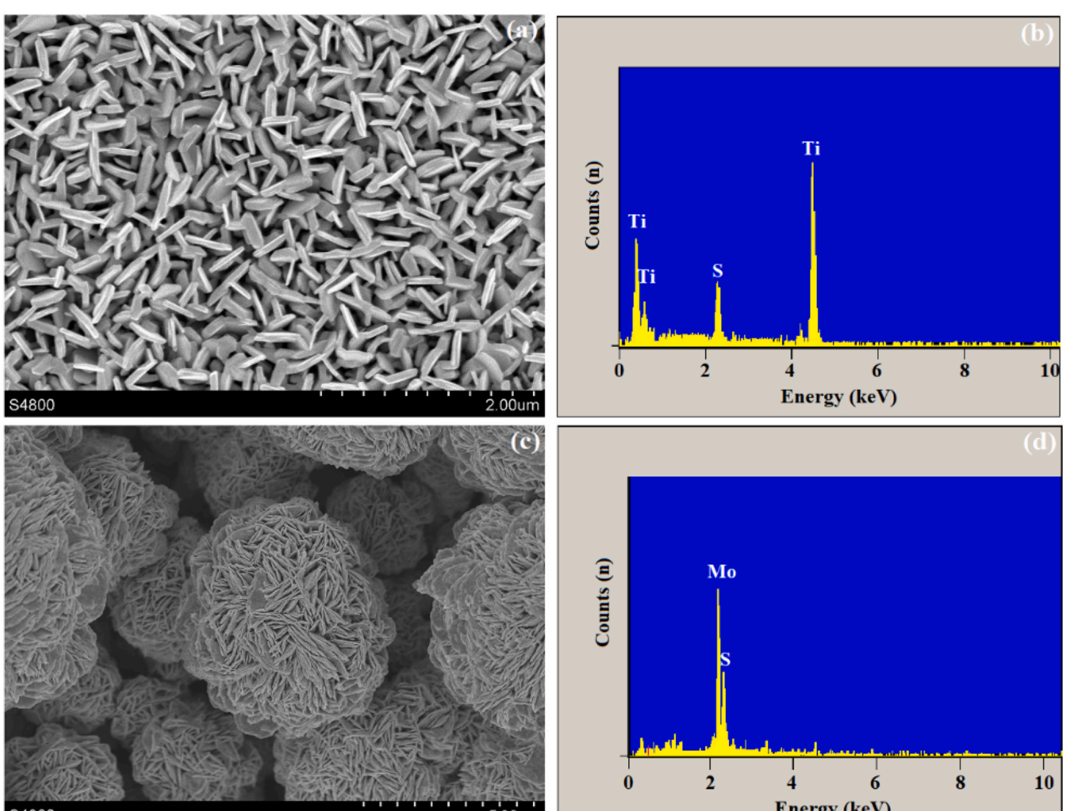

Fig. 4. (a) SEM of TiS_2 (b) EDX of TiS_2 (c) SEM of MoS_2 (d) EDX of MoS_2.

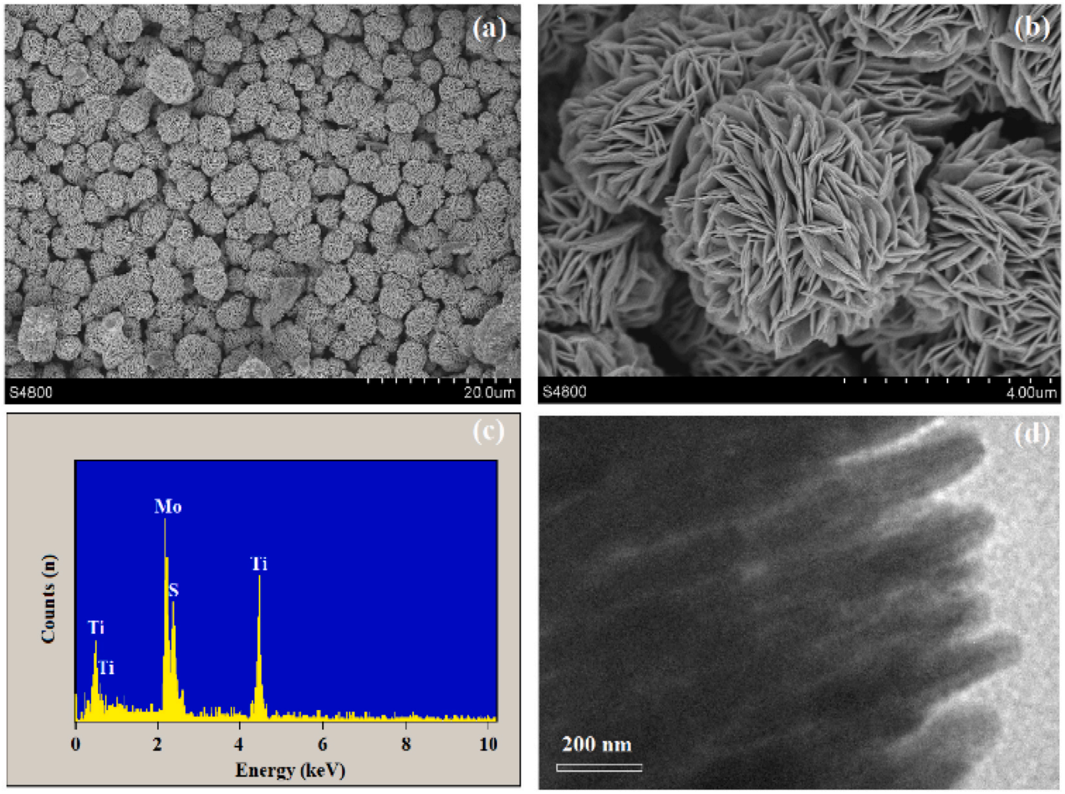

Fig. 5. (a) Low magnification TiS_2/MoS_2 composite SEM image (b) High magnification TiS_2/MoS_2 composite SEM image (c) EDS of TiS_2/MoS_2 composite (d) TEM of TiS_2/MoS_2 composite.

in Fig. 4 (b). Elemental analysis showing the controlled growth of TiS_2. The SEM image of synthesized MoS_2 have been shown in Fig. 4 (c) which are like micro spheres. The size of the individual microsphere is ranging from 3 to 5 μm and several nano-sheets like structures are observed on their surface. The size of the nanosheets is in nanometer range. Such microspheres with numerous sheets increases the roughness and finally the surface area which is crucial for the enhancement of the electrode performance. The EDS of MoS_2 is depicted in the Fig. 4 (d) showing that it consists of only Mo and S without any impurity. Smooth and pure materials are essential for the better performance.

The SEM of TiS_2/MoS_2 composite materials have been shown in the Fig. 5. The Fig. 5 (a) shows the low magnification image whereas Fig. 5 (b) shows the high magnification images. The Fig. 5 (a) clearly shows that the TiS_2/MoS_2 composite materials exhibit a relatively uniform size distribution of hierarchal micro-flowers with no agglomeration. In this TiS_2/MoS_2 composite materials apparently the TiS_2 micro rods are uniformly developed and distributed on MoS_2 spherical structure with sheets, which resultantly increases the ratio of the nano-sheets. The combination of sphere and nano-sheets form hierarchal micro-flowers as shown Fig. 5 (a, b). The size of these hierarchal micro-flowers is ranging from 2 to 4 μm which can be clearly seen in the Fig. 5 (a, b). This clearly reveals that the composite materials have smaller size as compared to

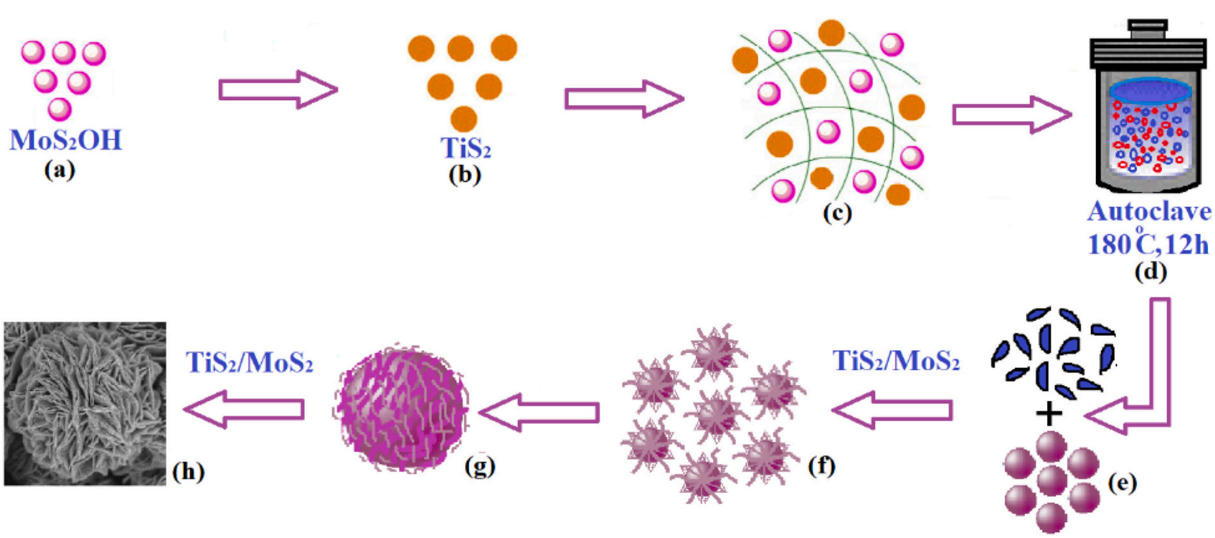

Fig. 6. Proposed growth mechanism of TiS_2/MoS_2 composite.

individual materials confirming the high surface area of the composite materials. Such composites presumably combination of two materials enhance the rough and surface area of the materials. Researchers have already demonstrated that a reduce size and higher diffusion will improve the surface area, that is extremely critical for improving capacitive properties and their stability. Furthermore, TiS_2/MoS_2 composite consisting of hierarchal micro-flowers structure, expanded porousness and high surface area delivers additional ways for ions transportation and direct interaction with active materials to enhance the capacitance performance. So, possibly with enhanced surface area these materials will improve the active regions and redox reaction reliability for better electrode performance. The EDS spectra of this composite was also analyzed and depicted in the Fig. 5 (c). The EDS spectra confirms the presence of Ti, M, and S, as well as the absence of any other peak demonstrating that the prepared samples are well synthesized. The peaks intensity also shows the systematic combination of TiS_2 and MoS_2.

Transmission electron microscopy is a sophisticated technique to analyze the dimensions and nature of the samples. The TEM of the TiS_2/MoS_2 composite materials is shown in the Fig. 5 (d). The TEM images clearly showing the nanosheets/rods like structures are present on the surface of the microspheres. In the TEM image, the size of nanosheets under observation can be seen clearly ranging from 85 to 120 nm. The TEM results are consistent with the SEM images as shown in Fig. 5 (b). Such smaller size and regular pattern/ regular structures are crucial for electrode materials.

Having intentions to investigate the possible growth progression of TiS_2/MoS_2 hierarchal micro-flowers, a number of experiments were performed and the resultant brief growth mechanism is depicted in Fig. 6. Under the suitable hydrothermal conditions and effective concentration gradient the ions and molecules are stimulated and carried to the growing area Fig. 6 (a, b, and c). in this process, MoS_2OH were dissolve in distilled water which further separate hydroxyl ion (OH^-) as shown in Eq. (3).

$$MoS_2OH + e- \rightarrow MoS_2 + OH- \tag{3}$$

The source of sulfur (H_2NCSNH_2) is very responsive to coordinate the molybdate as ($-NH_2$) is reductive functional group in source of sulfur which can easily react with the atomic molybdate. In continuation, the nuclei of MoS_2 are formed as a result of the reaction between sulfur and residual molybdenum. The lately grown MoS_2 nuclei have tendency to accumulate forming bigger particles which will definitely decrease their surface free energy, following the principle of Ostwald ripening as depicted in Fig. 6 (d, e, f, g, h) [32–34].

As preliminarily growth of MoS_2/TiS_2 hierarchal micro-flowers, the nano-sheets were fashioned with the evolution of the sheet planes and then stacking of layers on surface as in Fig. 6 (g, h). Some hierarchal flower-like MoS_2/TiS_2 microspheres appeared at prolonged (2 h) reaction time. The evolution process of hierarchal micro-flowers of MoS_2/TiS_2 initiates by nuclei which later developed into mature hierarchal micro-flowers like structures with sheets like structure which are clearly seen in Fig. 6 (f, g and h). In other possible growth mechanism, it has been proposed that with suitable concentration, time and temperature the dissolution of irregular nanorods/particles occur as a result the emerging petal-like (sheet-like) layer on the surface of the larger sphere are seemed carried out synchronously. The irregular growth of the sheets on the surface is attributed to the stress, Van der Waals interlayer interactions and local stacking along highest growth rate of the plane. The growth process activates with the initial nucleus growth process, then growth of nano-sheets and self-assembly growth process followed by a complete growth of hierarchical micro-spheres consistent with the Ostwald ripening process [64,65].

The other possible growth of such structures is attributed to the self-assembling directed by their intrinsic crystal orientation growth as larger structures will have large specific surface area. In the solution the ions can selectively absorb on their surface and their surface edges tends to vanish attributed to electron shielding effect [39]. So, numerous combinations of edges and surfaces will result hierarchal micro-flowers like microspheres having sheets on their surface which definitely increase their surface area tending high supercapacitor performance [65].

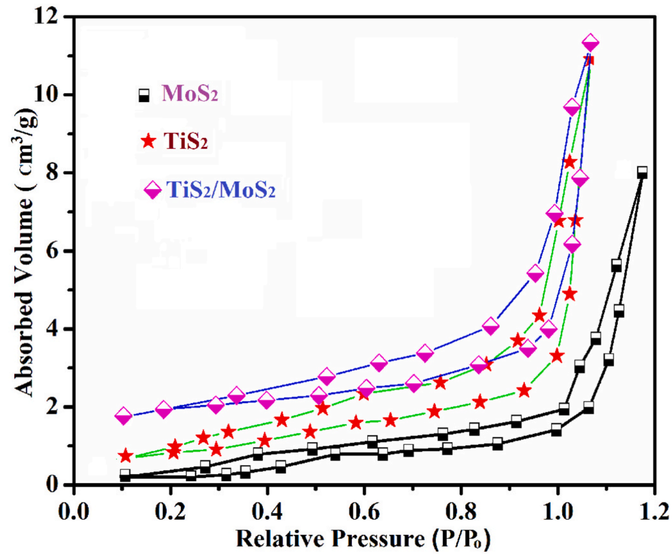

Fig. 7. N_2 adsorption–desorption isotherms of pure MoS_2, TiS_2, and TiS_2/MoS_2 samples.

Brunauer–Emmett–Teller (BET) theory is a sophisticated analysis technique used to measure the specific surface area of porous and solid materials. It gives crucial details about their physical structure. The surface areas of prepared samples were measured through BET technique by means of nitrogen (N_2) adsorption–desorption and the corresponding isotherms are shown in Fig. 7. The calculated surface areas of the pure MoS_2, TiS_2 and TiS_2/MoS_2 samples are 7.56, 9.6, and 13.1 m^2/g. It can be observed that surface area increased from 7.56 m^2/g to 13.1 13.1 m^2/g. TiS_2/MoS_2 large surface area (13.1 m^2/g) led to more redox reaction and active sites resulting in enhanced electrochemical characteristics.

3.1. Electrochemical measurements

The electrochemical capacities of synthesized electrodes such as TiS_2, MoS_2 and TiS_2/MoS_2 electrodes were examined through CV and each graph were presented in Fig. 8 (a), (b) and (c) respectively. The CV shapes of undoped TiS_2 and TiS_2 / MoS_2 composites were depicted at scan rates 5, 10, 25, 50 and 75 mvs^{-1} within the actual potential range of (0–0.7) V in 2 M KOH electrolyte see Fig. 8 (a, b, c). Oxidation / reduction peaks were found in the CV graphs owing to pseudo capacitive behavior of prepared electrodes, and it were deduced that the charge on the surface of prepared electrodes is attributable to the redox process. In the CV curves, the TiS_2/MoS_2 composite electrode had greater integrated areas than the TiS_2 electrode, suggesting a significantly increased specific capacitance due to the integrated area. It has been observed that once scan rates rise, all CV curves take on a similar form, indicating the presence of pseudo capacitive characteristics.

Recently various composites have been studied and their different specific capacitance have been carried out, resulting AC/MoS_2 (261 F/g) [66], MoS_2@TiO_2 (210 F/g) [54], TiS_2/g-C_3N_4 (546 F/g) [50] and MoS_2/g-C3N4 (240.85 F/g) [30]. Specific capacitance of prepared electrodes MoS_2, TiS_2, and TiS_2/MoS_2 hierarchal micro-flowers composites have been measured at various scan rate (5, 10,25,50,75) by using Eq. (1). A higher specific capacitance 780 F/g as in Fig. 8 (d) was calculated from hybrid composites TiS_2/MoS_2 hierarchal micro-flowers combinations at the scan rate of 10 mV/s as compared to pristine TiS_2 have 480 F/g and MoS_2 has 402 F/g. The oxidation and reduction

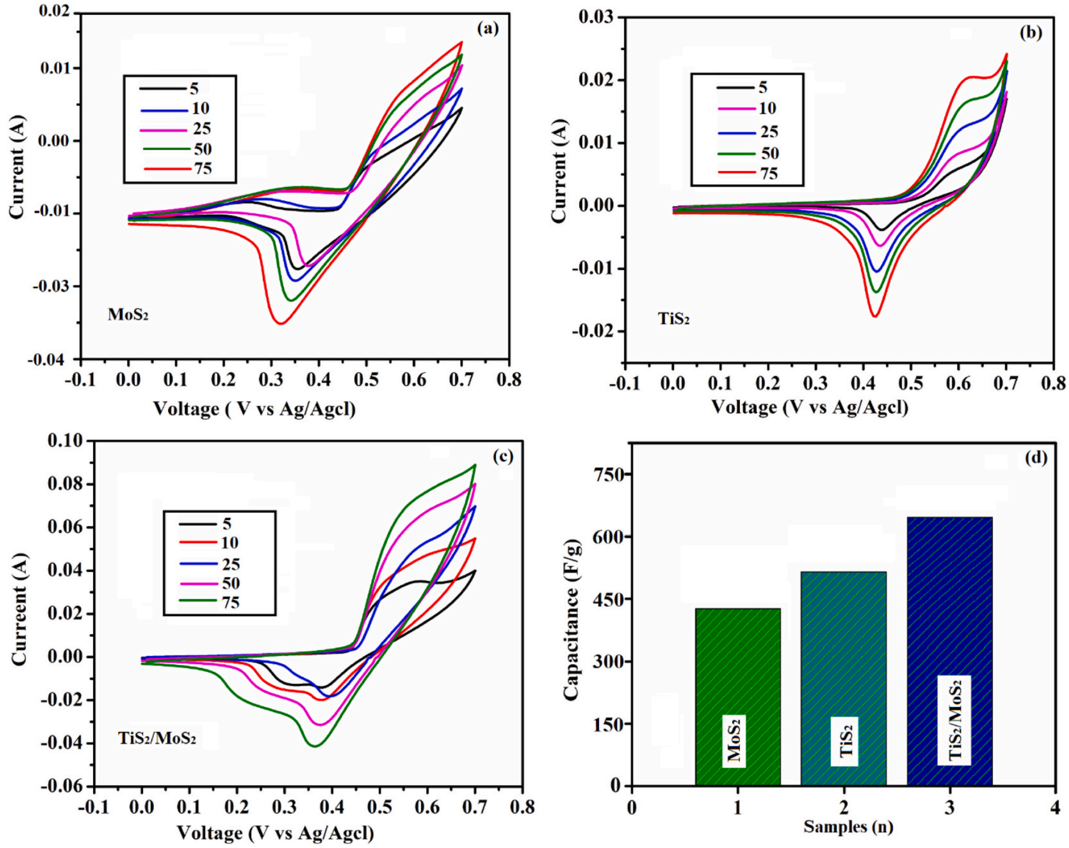

Fig. 8. (a) CV graph of TiS_2 (b) CV graph of MoS_2 (c) CV graph of TiS_2 / MoS_2 (d) Specific capacitance of TiS_2, MoS_2 and TiS_2 / MoS_2.

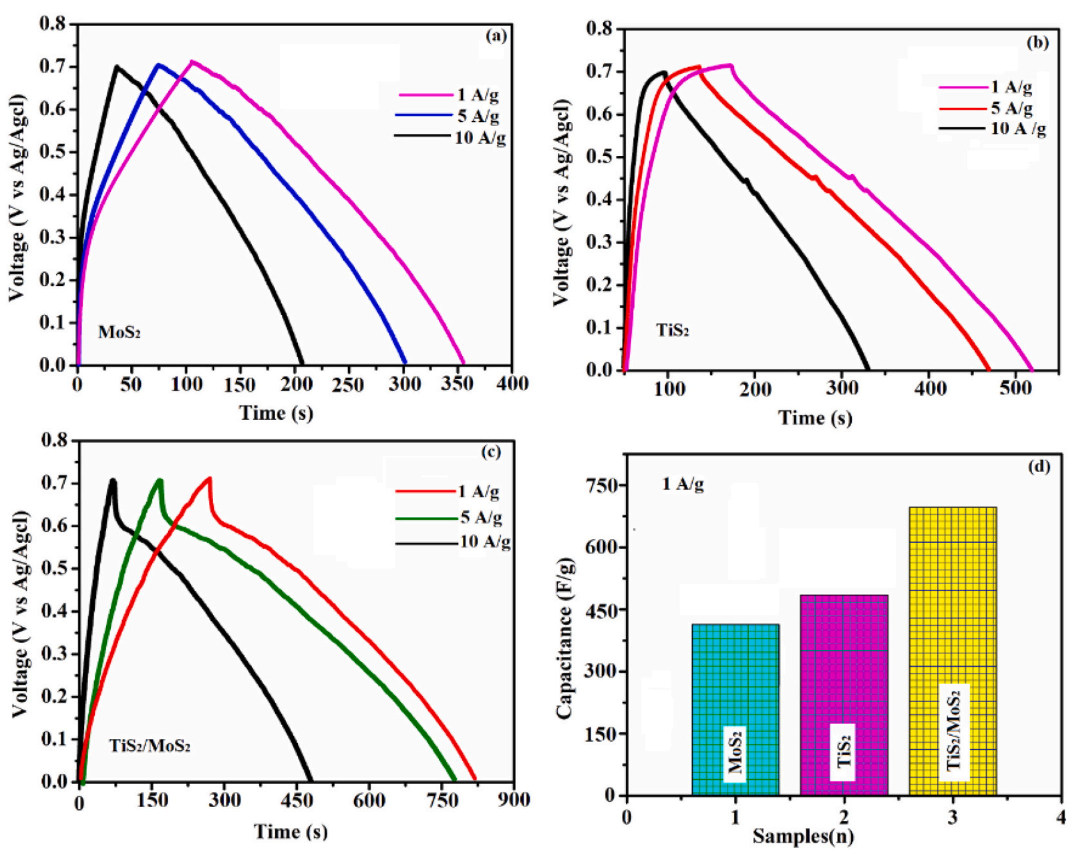

Fig. 9. (a) GCD curves of MoS_2 (b) GCD curves of TiS_2 (c) GCD curves of TiS_2/MoS_2 (d) Specific capacitance of TiS_2, MoS_2 and TiS_2/MoS_2 at 1 A/g.

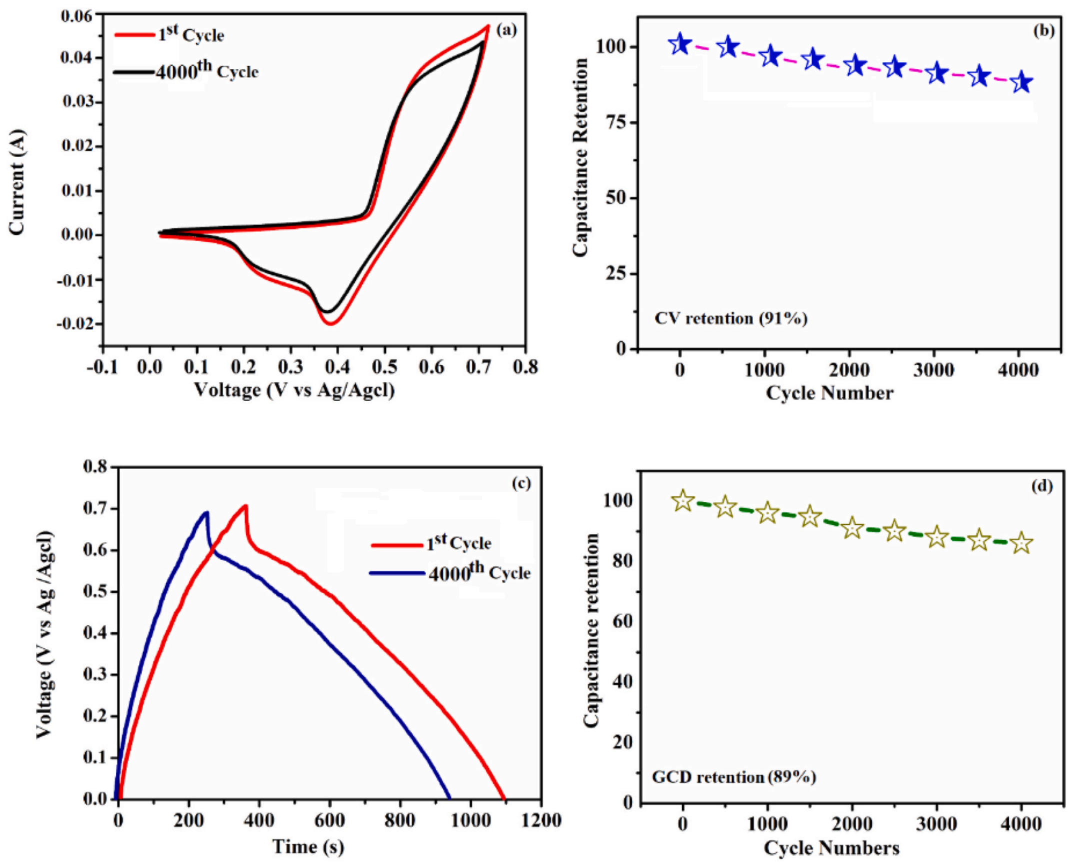

Fig. 10. (a) CV cyclic stability of TiS_2/MoS_2 (b) Cyclic stability retention (c) GCD cyclic stability of TiS_2/MoS_2 (d) GCD cyclic stability retention.

reactions of TiS_2 and MoS_2 in 2 M KOH electrolyte is given by Eqs. (4) and (5):

$$MoS_2 + OH^- \rightarrow MoS_2OH + e^- \quad (4)$$

$$TiS_2 + OH^- \rightarrow TiS_2OH + e^- \quad (5)$$

Due to the limitation of charge transfer rates and diffusion of the alkaline electrolyte throughout the quick reaction phase, the redox peaks frequently broadened.

For TiS_2, MoS_2 and TiS_2 / MoS_2 GCD graphs conceded at various 1, 5 and 10 A/g current densities which is shown in Fig. 9 (a, b, c). GCD curves shows the regular patterns and indicate a rather symmetric nature over the hypothetical span of 0 to 0.7 V. The generated electrode is said to have a better long-term behavior and redox reaction within the certain potential range. The specific capacitance of TiS_2, MoS_2 and TiS_2/MoS_2 at 1 A/g is 391, 462 and 701 F/g respectively as shown in Fig. 9 (d). Consistent with the CV findings, the graph shows an estimated mirror-like potential-time reaction characteristic, indicating that the charge/discharge mechanism of prepared electrodes is cyclic. Discharge curves are nonlinear which further confirms the prepared electrode is pseudo capacitor in nature. This potency related to the electrochemical adsorbent reaction at the electrode–electrolyte contact.

The speed of alkali ions spreading in and out by the electrolyte interface controls the discharge time of the prepared electrodes. The TiS_2/MoS_2 micro flower-composite electrode has a much higher discharge time than the TiS_2 and MoS_2 electrode. Higher redox reactions owing to much further adsorption sites and homogenous structure are ascribed to extended discharge period of TiS_2/MoS_2 hierarchal micro-

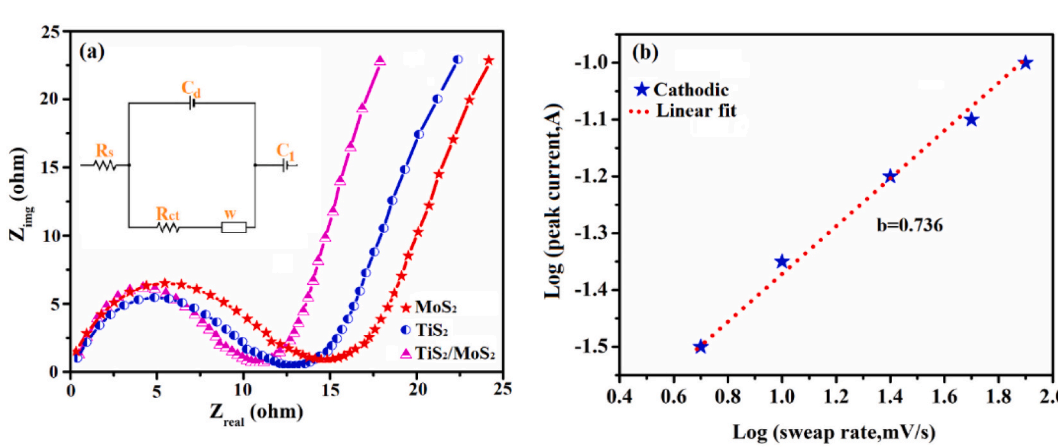

Fig. 11. (a) EIS of TiS_2, MoS_2 and TiS_2 / MoS_2 (b) log(V) vs log(i_p).

Table 1
Specific capacitance based comparison of various composite electrode materials.

S No	Electrode Materials	Method	Morphology	Scan rate / current density	Specific Capacitance	Ref
1.	AC/MoS_2	Hydrothermal	Nano-composites	2 mvs^{-1}	261 F/g	[66]
2.	MoS_2@ TiO_2	Hydrothermal	Binary-Composites	10 mvs^{-1}	210 F/g	[54]
3.	PANI/CNT/MoS_2	Polymerization	Ternary composites	01 Ag^{-1}	350 F/g	[67]
4.	TiS_2/g-C_3N_4	Hydrothermal	Micro-composites	10 mvs^{-1}	546 F/g	[50]
5.	MoS_2-g-C_3N_4	Mechanochemistry	Hetero structures	10 mvs^{-1}	240.85 F/g	[30]
6.	MoS_2/PPy-2	Hydrothermal	Nano-composite	10 mvs^{-1}	700 F/g	[68]
7.	MoS_2/PANI	Hydrothermal	Nanowire	0.5 Ag^{-1}	552 F/g	[69]
8.	MoS_2/RCF	Hydrothermal	Spheres	0.5 Ag^{-1}	225 F/g	[70]
9.	TiS_2/MoS_2	Hydrothermal	Hierarchal micro-flowers.	10 mvs^{-1}	709 F/g	This work

flowers electrode which is intensely approved with the structural and surface morphological description as in SEM images (Fig. 6 b).

Moreover, cycling stability of synthesized samples TiS_2/MoS_2 hierarchal micro-flowers composite nickel foam electrode (Fig. 10a) revealed that after 4000 cycles, 91 % (Fig. 10b) of the original capacitance was preserved, confirming the excellent cycle lifetime.

According to the results of the following electrochemical tests, the TiS_2/MoS_2 hierarchal micro-flowers composite demonstrated good capacitance and cycling stability performance at greater charging and discharge currents. There were primarily two explanations for this: (i) There were aggregation of TiS_2 with MoS_2 might improve the effective surface area, reducing atom size and providing additional active lattice sites in the hierarchal micro-flowers combinations, which is greatest suited for oxidation and reduction. (ii) TiS2 provides additional channels for electron and ion transportation, improving the TiS_2/MoS_2 composite electrode electric conductivity. The TiS_2/MoS_2 composite electrode capacitance and cycle performance were improved synergistically by its reduced size, good electrical conductivity, and remarkable diffusing mode. As a result, TiS_2/MoS_2 electrode composite is a promising applicant for supercapacitor applications. Interestingly, after 4000 GCD cycles (Fig. 10c), this electrode material retained 91 % (Fig. 10d) percent of its charge, suggesting long-term cycling.

Regardless of reasonable stability and excellent capacitance retention, the electrode material should retain decent electrochemical kinetics. Electrochemical impedance spectroscopy (EIS) is a comprehensive tool for studying electrochemical kinetics phenomena in more detail. The EIS results of prepared samples of $TiS_{2,}$ MoS_2 and TiS_2/MoS_2 composites electrodes are mentioned in Fig. 11 (a) as a Nyquist graph. TiS_2 exhibits a broad and depressed semicircle at the higher frequency zone and a nearly linear in the lower frequency area, indicating a significant charge transmission resistance as shown in Fig. 11 (a). Here in the Nyquist plots the real and imaginary component of EIS are depicted in Fig. 11 (a). The semicircle is crucial parameter associated with the electron transfer at the electrolyte / electrode boundary (resistance) interface, that is suitable to improves the conductivity. In the Nyquist plot the semicircle is associated with the electrical conductivity whereas it's slop (linear part) is related to the charge transfer resistance. Usually the equivalent series resistance (ESR) is estimated through the intersection of the curve at x-axis [71].

As compared to pristine samples, the smaller semicircle of TiS_2/MoS_2 composite exhibited the lower charge transfer resistance. This will provide good conductivity following excellent activity and charges transfer resulting high capacitance. The vertical line behavior of TiS_2/MoS_2 composite at lower frequency also confirmed the specified rapid ion diffusion in the electrode surface [72].

Inset of the Fig. 11(a) is the EIS equivalent circuit diagram.

In addition, the “b” value calculated in Fig. 11 (b) using power law, and its parameter that provides evidence on electrochemical performance, was evaluated to be “b = 0.736”. This “b” value, which is higher than 0.5 and closer to near 1, once again confirming that as synthesized electrode TiS_2/MoS_2 material has capacitive nature. The electrochemical study of the synthesized samples and their comparison based on specific capacitance (Table 1) and stability, revealed that the combination TiS_2/MoS_2 hierarchal micro-flowers displayed excellent capacitive and cycling properties, suggesting that it's a great choice for potential applications for supercapacitor electrodes.

4. Conclusion

The TiS_2/MoS_2 composite has been successfully synthesized by facile hydrothermal technique that effectively prevented aggregation. The incorporation of TiS_2 to MoS_2 shows a vital role in separating and reducing the composite material size. TiS_2/MoS_2 composites reveals a higher specific capacitance of 709 F/g at the scan rate of 10 mV/s, that is considerably much higher than TiS_2 and MoS_2 separately as well as other reported materials. The synergetic effect of declining charge transmission resistance and improving charge diffusion rate has been ascribed to the substantial improvement in ionic conductivity. The TiS_2/MoS_2 composite also retained 91 % of its strength after 4000 cycles, demonstrating its exceptional stability. As a result, the prepared electrode materialTiS_2/MoS_2 is a feasible for supercapacitor electrode materials applications.

CRediT authorship contribution statement

Ghulam Nabi: Conceptualization, Supervision, Resources, Writing.
Wajid Ali: Methodology, Investigation, Writing.
Muhammad Tanveer: Formal Analysis, Data Curation, Writing.
Tahir Iqbal: Review & Editing.
Muhammad Rizwan: Writing, Revision.
S. Hussain: Review & Editing, Resources.

Declaration of competing interest

The authors declare that they have no known competing financial interests or personal relationships that could have appeared to influence the work reported in this paper.

Data availability

No data was used for the research described in the article.

Acknowledgement

The authors (Dr. Ghulam Nabi and Dr. Tahir Iqbal) extend their appreciation to Higher Education Commission (HEC) of Pakistan for NRPU Research Project No. 14755.

References

[1] W. Raza, et al., Recent advancements in supercapacitor technology, Nano Energy 52 (2018) 441–473.
[2] M.B. Poudel, G.P. Ojha, H.J. Kim, Manganese-doped tungsten disulfide microcones as binder-free electrode for high performance asymmetric supercapacitor, J. Energy Storage 47 (2022) 103674.

[3] L. Zhang, et al., A review of supercapacitor modeling, estimation, and applications: a control/management perspective, Renew. Sust. Energ. Rev. 81 (2018) 1868–1878.
[4] R. Ahmed, G. Nabi, Enhanced electrochemical performance of Cr-doped NiO nanorods for supercapacitor application, J.Energy Storage 33 (2021), 102115.
[5] W. Zuo, et al., Battery-supercapacitor hybrid devices: recent progress and future prospects, Adv.Sci. 4 (7) (2017), 1600539.
[6] R. Ahmed, G. Nabi, Morphology tailoring and enhanced electrochemical properties of Cd–Zn co-doped NiO nanorods for high performance supercapacitor, Ceram. Int. 46 (14) (2020) 22330–22337.
[7] L. Fan, et al., A nonaqueous potassium-based battery–supercapacitor hybrid device, Adv. Mater. 30 (20) (2018), 1800804.
[8] A. Borenstein, et al., Carbon-based composite materials for supercapacitor electrodes: a review, J. Mater. Chem. A 5 (25) (2017) 12653–12672.
[9] N. Choudhary, et al., Asymmetric supercapacitor electrodes and devices, Adv. Mater. 29 (21) (2017), 1605336.
[10] K.S. Kumar, et al., Recent advances in two-dimensional nanomaterials for supercapacitor electrode applications, ACS Energy Lett. 3 (2) (2018) 482–495.
[11] H. Yang, Effects of supercapacitor physics on its charge capacity, IEEE Trans. Power Electron. 34 (1) (2018) 646–658.
[12] G.G. Prasad, et al., Supercapacitor technology and its applications: a review, in: IOP Conference Series: Materials Science and Engineering, IOP Publishing, 2019.
[13] E.E. Miller, Y. Hua, F.H. Tezel, Materials for energy storage: review of electrode materials and methods of increasing capacitance for supercapacitors, J.Energy Storage 20 (2018) 30–40.
[14] X. Feng, et al., Integrated energy storage system based on triboelectric nanogenerator in electronic devices, Front. Chem. Sci. Eng. 15 (2) (2021) 238–250.
[15] J. Libich, et al., Supercapacitors: properties and applications, J.Energy Storage 17 (2018) 224–227.
[16] L. Wang, et al., Hybrid model predictive control strategy of supercapacitor energy storage system based on double active bridge, Energies 12 (11) (2019) 2134.
[17] P. Golchoubian, N.L. Azad, Real-time nonlinear model predictive control of a battery–supercapacitor hybrid energy storage system in electric vehicles, IEEE Trans. Veh. Technol. 66 (11) (2017) 9678–9688.
[18] P. Singh, J. Bahadur, K. Pal, One-step one chemical synthesis process of graphene from rice husk for energy storage applications, Graphene 6 (3) (2017) 61–71.
[19] L. Kouchachvili, W. Yaïci, E. Entchev, Hybrid battery/supercapacitor energy storage system for the electric vehicles, J. Power Sources 374 (2018) 237–248.
[20] H. Yang, Analysis of supercapacitor charge redistribution through constant power experiments, in: 2017 IEEE Power & Energy Society General Meeting, IEEE, 2017.
[21] C. Zequine, et al., High-performance flexible supercapacitors obtained via recycled jute: bio-waste to energy storage approach, Sci. Rep. 7 (1) (2017) 1–12.
[22] M. Cakici, R.R. Kakarla, F. Alonso-Marroquin, Advanced electrochemical energy storage supercapacitors based on the flexible carbon fiber fabric-coated with uniform coral-like MnO2 structured electrodes, Chem. Eng. J. 309 (2017) 151–158.
[23] Y.A. Kumar, H.-J. Kim, Preparation and electrochemical performance of NiCo 2 O 4@ NiCo 2 O 4 composite nanoplates for high performance supercapacitor applications, New J. Chem. 42 (24) (2018) 19971–19978.
[24] Z. Zhao, et al., Multifunctional transitional metal-based phosphide nanoparticles towards improved polysulfide confinement and redox kinetics for highly stable lithium-sulfur batteries, Chem. Eng. J. 450 (2022), 138310.
[25] A. Afif, et al., Advanced materials and technologies for hybrid supercapacitors for energy storage–a review, J.Energy Storage 25 (2019), 100852.
[26] A.K. Yedluri, et al., Facile synthesis of novel and highly efficient CoNi2S4-Ni (OH) 2 nanosheet arrays as pseudocapacitive-type electrode material for high-performance electrochemical supercapacitors, J.Energy Storage 31 (2020), 101623.
[27] H. Li, et al., Microstructure controlled synthesis of Ni, N-codoped CoP/carbon fiber hybrids with improving reaction kinetics for superior sodium storage, J.Mater.Sci. Technol. 99 (2022) 184–192.
[28] T. Salameh, et al., Integrated standalone hybrid solar PV, fuel cell and diesel generator power system for battery or supercapacitor storage systems in Khorfakkan, United Arab Emirates, Int. J. Hydrog. Energy 46 (8) (2021) 6014–6027.
[29] X. Cheng, et al., Nanoconfined SnS2 in robust SnO2 nanocrystals building heterostructures for stable sodium ion storage, Chem. Eng. J. 442 (2022), 136222.
[30] S.A. Ansari, M.H. Cho, Simple and large scale construction of MoS2-g-C3N4 heterostructures using mechanochemistry for high performance electrochemical supercapacitor and visible light photocatalytic applications, Sci. Rep. 7 (1) (2017) 1–11.
[31] Z. Zhao, et al., Synergetic effect of spatially separated dual co-catalyst for accelerating multiple conversion reaction in advanced lithium sulfur batteries, Nano Energy 81 (2021), 105621.
[32] S. Tian, X. Zhang, Z. Zhang, Capacitive deionization with MoS2/g-C3N4 electrodes, Desalination 479 (2020), 114348.
[33] Y.A. Kumar, K.D. Kumar, H.-J. Kim, A novel electrode for supercapacitors: efficient PVP-assisted synthesis of Ni 3 S 2 nanostructures grown on Ni foam for energy storage, Dalton Trans. 49 (13) (2020) 4050–4059.
[34] J. Wang, et al., Recent progress in micro-supercapacitor design, integration, and functionalization, Small Methods 3 (8) (2019), 1800367.
[35] H. Dou, et al., Revisiting the degradation of solid/electrolyte interfaces of magnesium metal anodes: decisive role of interfacial composition, Nano Energy 86 (2021), 106087.
[36] Z. Zhao, et al., Understanding the modulation effect and surface chemistry in a heteroatom incorporated graphene-like matrix toward high-rate lithium–sulfur batteries, Nanoscale 13 (35) (2021) 14777–14784.
[37] I. Hussain, et al., Uniform growth of ZnS nanoflakes for high-performance supercapacitor applications, J.Energy Storage 36 (2021), 102408.
[38] J. Guo, et al., Double-shell CuS nanocages as advanced supercapacitor electrode materials, J. Power Sources 355 (2017) 31–35.
[39] I.Y. Bu, R. Huang, Fabrication of CuO-decorated reduced graphene oxide nanosheets for supercapacitor applications, Ceram. Int. 43 (1) (2017) 45–50.
[40] B. Guan, et al., Synthesis of hierarchical NiS microflowers for high performance asymmetric supercapacitor, Chem. Eng. J. 308 (2017) 1165–1173.
[41] M.A. Bissett, et al., Comparison of two-dimensional transition metal dichalcogenides for electrochemical supercapacitors, Electrochim. Acta 201 (2016) 30–37.
[42] T. Liu, et al., Hierarchical NiS/N-doped carbon composite hollow spheres with excellent supercapacitor performance, J. Mater. Chem. A 5 (40) (2017) 21257–21265.
[43] M. Moniruzzaman, et al., Two-dimensional core-shell structure of cobalt-doped@ MnO2 nanosheets grown on nickel foam as a binder-free battery-type electrode for supercapacitor application, Nanomaterials 12 (18) (2022) 3187.
[44] P. Ji, et al., Ti-doped tunnel-type Na4Mn9O18 nanoparticles as novel anode materials for high-performance supercapacitors, ACS Appl. Mater. Interfaces 11 (32) (2019) 28900–28908.
[45] Y. Zeng, et al., Advanced Ti-doped Fe2O3@ PEDOT core/shell anode for high-energy asymmetric supercapacitors, Adv. Energy Mater. 5 (12) (2015), 1402176.
[46] P.H. Jampani, et al., High energy density titanium doped-vanadium oxide-vertically aligned CNT composite electrodes for supercapacitor applications, J. Mater. Chem. A 3 (16) (2015) 8413–8432.
[47] A. Ali, et al., Mo-doped ZnO nanoflakes on Ni-foam for asymmetric supercapacitor applications, RSC Adv. 9 (47) (2019) 27432–27438.
[48] A.M. Elshahawy, et al., Sulfur-doped cobalt phosphide nanotube arrays for highly stable hybrid supercapacitor, Nano Energy 39 (2017) 162–171.
[49] X. Chang, et al., MnO2/g-C3N4 nanocomposite with highly enhanced supercapacitor performance, Nanotechnology 28 (13) (2017), 135705.
[50] G. Nabi, et al., Cogent synergic effect of TiS2/g-C3N4 composite with enhanced electrochemical performance for supercapacitor, Ceram. Int. 46 (17) (2020) 27601–27607.
[51] A. Chaturvedi, et al., Unveiling two-dimensional TiS 2 as an insertion host for the construction of high energy Li-ion capacitors, J. Mater. Chem. A 5 (19) (2017) 9177–9181.
[52] M. Tobis, S. Sroka, E. Frąckowiak, Supercapacitor with carbon/MoS2 composites, Front. Energy Res. 9 (2021), 647878.
[53] S. Hou, et al., Construction of ball-flower like NiS2@ MoS2 composite for high performance supercapacitors, Electrochim. Acta 330 (2020), 135208.
[54] M. Iqbal, et al., High-performance supercapacitor based on MoS2@ TiO2 composite for wide range temperature application, J. Alloys Compd. 883 (2021), 160705.
[55] Q. Liao, et al., Interfacial bonding enhancement and properties improvement of carbon/copper composites based on nickel doping, Compos. Interfaces 28 (6) (2021) 637–649.
[56] Y.A. Kumar, et al., A MoNiO 4 flower-like electrode material for enhanced electrochemical properties via a facile chemical bath deposition method for supercapacitor applications, New J. Chem. 44 (2) (2020) 522–529.
[57] D.K. Kulurumotlakatla, A.K. Yedluri, H.-J. Kim, Hierarchical NiCo2S4 nanostructure as highly efficient electrode material for high-performance supercapacitor applications, J.Energy Storage 31 (2020), 101619.
[58] Y. Cao, et al., Metal/porous carbon composites for heterogeneous catalysis: old catalysts with improved performance promoted by N-doping, ACS Catal. 7 (12) (2017) 8090–8112.
[59] L. Ao, et al., Superior and reversible lithium storage of SnO2/graphene composites by silicon doping and carbon sealing, ACS Appl. Mater. Interfaces 12 (18) (2020) 20824–20837.
[60] A.K. Yedluri, H.-J. Kim, Wearable super-high specific performance supercapacitors using a honeycomb with folded silk-like composite of NiCo 2 O 4 nanoplates decorated with NiMoO 4 honeycombs on nickel foam, Dalton Trans. 47 (43) (2018) 15545–15554.
[61] M.R. Pallavolu, et al., Facile fabrication of novel heterostructured tin disulfide (SnS2)/tin sulfide (SnS)/N-CNO composite with improved energy storage capacity for high-performance supercapacitors, J. Electroanal. Chem. 899 (2021), 115695.
[62] M.S. Whittingham, Lithium titanium disulfide cathodes, Nat. Energy 6 (2) (2021), 214-214.
[63] Y.A. Kumar, K.D. Kumar, H.-J. Kim, Facile preparation of a highly efficient NiZn 2 O 4–NiO nanoflower composite grown on Ni foam as an advanced battery-type electrode material for high-performance electrochemical supercapacitors, Dalton Trans. 49 (11) (2020) 3622–3629.
[64] P.W. Voorhees, The theory of Ostwald ripening, J. Stat. Phys. 38 (1) (1985) 231–252.
[65] X. Zheng, et al., Hydrothermal synthesis of MoS2 with different morphology and its performance in thermal battery, J. Power Sources 395 (2018) 318–327.
[66] D. Sangeetha, M. Selvakumar, Active-defective activated carbon/MoS2 composites for supercapacitor and hydrogen evolution reactions, Appl. Surf. Sci. 453 (2018) 132–140.
[67] A.K. Thakur, et al., Facile synthesis and electrochemical evaluation of PANI/CNT/MoS2 ternary composite as an electrode material for high performance supercapacitor, Mater. Sci. Eng. B 223 (2017) 24–34.
[68] X.-Q. Li, et al., Research on carbon-based electrode materials for supercapacitors, Acta Phys. -Chim. Sin. 33 (1) (2017) 130–148.
[69] I.-W.P. Chen, Y.-C. Chou, P.-Y. Wang, Integration of ultrathin MoS2/PANI/CNT composite paper in producing all-solid-state flexible supercapacitors with

exceptional volumetric energy density, J. Phys. Chem. C 123 (29) (2019) 17864–17872.
[70] C. Zhao, et al., Facile construction of MoS2/RCF electrode for high-performance supercapacitor, Carbon 127 (2018) 699–706.
[71] H. Liu, et al., Doping cobalt hydroxide nanowires for better supercapacitor performance, Acta Mater. 84 (2015) 20–28.
[72] Y. Bai, et al., Supercapacitors with high capacitance based on reduced graphene oxide/carbon nanotubes/NiO composite electrodes, J. Mater. Chem. A 2 (11) (2014) 3834–3840.